Flagellar perturbations activate adhesion through two distinct pathways in *Caulobacter crescentus*

David M. Hershey[2], Aretha Fiebig[1] and Sean Crosson[1] #

[1] Department of Microbiology and Molecular Genetics, Michigan State University, East Lansing, MI 48824, USA

[2] Department of Biochemistry and Molecular Biology, University of Chicago, Chicago, IL 60637, USA

Running title: Flagellar signaling in *C. crescentus*

To whom correspondence should be addressed: crosson4@msu.edu; (517) 884-5345

Keywords: Adhesion, flagellum, motility, holdfast, biofilm

Abstract: Bacteria carry out sophisticated developmental programs to colonize exogenous surfaces. The rotary flagellum, a dynamic machine that drives motility, is a key regulator of surface colonization. The specific signals recognized by flagella and the pathways by which those signals are transduced to coordinate adhesion remain subjects of debate. Mutations that disrupt flagellar assembly in the dimorphic bacterium *Caulobacter crescentus* stimulate the production of a polysaccharide adhesin called the holdfast. Using a genome-wide phenotyping approach, we compared surface adhesion profiles in wild-type and flagellar mutant backgrounds of *C. crescentus*. We identified a diverse set of flagellar mutations that enhance adhesion by inducing a hyper-holdfast phenotype and discovered a second set of mutations that suppress this phenotype. Epistasis analysis of the *flagellar signaling suppressor* (*fss*) mutations demonstrated that the flagellum stimulates holdfast production via two genetically distinct pathways. The developmental regulator PleD contributes to holdfast induction in mutants disrupted at both early and late stages of flagellar assembly. Mutants disrupted at late stages of flagellar assembly, which assemble an intact rotor complex, induce holdfast production through an additional process that requires the MotAB stator and its associated diguanylate cyclase, DgcB. We have assigned a subset of the *fss* genes to either the stator- or *pleD*-dependent networks and characterized two previously unidentified motility genes that regulate holdfast production via the stator complex. We propose a model through which the flagellum integrates mechanical stimuli into the *C. crescentus* developmental program to coordinate adhesion.

Importance: Understanding how bacteria colonize solid surfaces is of significant clinical, industrial and ecological importance. In this study, we identified genes that are required for *Caulobacter crescentus* to activate surface attachment in response to signals from a macromolecular machine called the flagellum. Genes involved in transmitting information from

40 the flagellum can be grouped into separate pathways, those that control the *C. crescentus*
41 morphogenic program and those that are required for flagellar motility. Our results support a
42 model in which a developmental and a mechanical signaling pathway operate in parallel
43 downstream of the flagellum and converge to regulate adhesion. We conclude that the flagellum
44 serves as a signaling hub by integrating internal and external cues to coordinate surface
45 colonization and emphasize the role of signal integration in linking complex sets of environmental
46 stimuli to individual behaviors.
47
48 **Introduction:** For microorganisms, solid surfaces serve as sites of nutrient accumulation,
49 gateways into host tissues and shelters from environmental stresses (1–3). To access surface-
50 associated niches, bacteria deploy specialized programs for seeking, recognizing and colonizing
51 objects in their surroundings (4). These programs culminate in a pronounced transition away
52 from a free-living, exploratory state and toward an adherent, sessile lifestyle (5–7). Sophisticated
53 signaling networks that integrate a host of environmental cues are used to coordinate the motile-
54 to-sessile switch (8–10). The complexity of these circuits reflects the perilous nature of
55 committing to colonization programs under sub-optimal conditions.
56 A transenvelope machine called the flagellum drives cellular motility and plays a critical
57 role at numerous stages of surface colonization(11, 12). The flagellum is synthesized in a stepwise
58 process that is controlled by a transcriptional hierarchy(13). Assembly begins with the expression
59 of class II genes that code for a rotor and secretion subcomplex that are inserted in the
60 cytoplasmic membrane(14, 15). Upon completion of the class II program, assembly proceeds
61 outward with the incorporation of an envelope spanning basal body (class III genes) followed by
62 the secretion of an extracellular filament (class IV genes) (16, 17). Stator subcomplexes that
63 surround the rotor utilize ion gradients across the cytoplasmic membrane to generate torque by

64 turning the hook-basal body complex and its associated filament, propelling the cell forward (Fig
65 1)(18, 19). Flagellar motors are highly attuned to environmental conditions. They support motility
66 under diverse conditions, modulate torque in response to changing loads and alter rotational bias
67 to support complex swimming patterns(20–23).

68 Paradoxically, flagellar motility must be repressed during sessile growth but is also
69 required for efficient surface colonization(6, 24–26). During the initial stages of attachment,
70 swimming is thought to promote productive interactions with target substrates by providing
71 energy needed to overcome repulsive forces at the liquid-solid interface(27). The flagellum also
72 plays an additional regulatory role in activating the motile-to-sessile transition by recognizing
73 physical contact with solid substrates(11). Such tactile sensing events serve as critical cues for
74 initiating colonization programs, but the mechanistic basis for how bacteria sense and respond to
75 physical stimuli remains controversial.

76 The dimorphic bacterium *Caulobacter crescentus* is uniquely adapted to surface
77 colonization. Cell division in *C. crescentus* is asymmetric and yields to two distinct cell types(28).
78 Newborn swarmer cells are flagellated, produce type IV pili (T4P) and cannot initiate replication
79 (29, 30). These motile cells undergo a morphogenic transition to become replication-competent
80 stalked cells by replacing their flagellum and pili with a specialized envelope extension called the
81 stalk(31). During the swarmer-to-stalked transition, *C. crescentus* can produce a polysaccharide
82 adhesin called the holdfast that is displayed at the tip of the stalked cell where it promotes
83 attachment to surfaces (Fig 1) (7, 32). Holdfast production is the primary determinant of surface
84 colonization in *C. crescentus,* and its regulation is elaborate (26, 33). In addition to cell cycle
85 cues(7, 34), nutrient availability(35), light(36) and redox status(37), mechanical contact has been
86 implicated as an important activator of holdfast assembly (38). Recent evidence suggests that both
87 flagella and T4P can stimulate holdfast production in response to contact with a surface(39, 40),

88 but conflicting models have emerged for how these transenvelope machines survey and
89 disseminate mechanical information(34, 41).

90 Here, we used an unbiased phenotyping approach called adhesion profiling to show that a
91 diverse set of flagellar mutations induce a hyper-holdfast phenotype and to identify dozens of
92 *flagellar signaling suppressor* (*fss*) genes that contribute to holdfast stimulation downstream of the
93 flagellum. *fss* mutations suppress the hyper-adhesive effects of flagellar disruption through two
94 distinct pathways. Select regulators of cell-cycle progression are involved in stimulating adhesion
95 upon flagellar disruption, while components of the stator subcomplexes contribute to holdfast
96 stimulation specifically in mutants that can assemble an inner membrane rotor. We assigned roles
97 for two previously uncharacterized genes roles in the stator-dependent pathway and
98 demonstrated that they promote the ability of the stator subunits to turn the flagellar filament.
99 Our results provide new insight into load sensing by the *C. crescentus* motor and highlight a novel
100 link between flagellar assembly and morphogenesis. We propose a broad role for the flagellum in
101 coordinating cellular physiology through its role as a signaling hub that integrates internal and
102 external cues.

103

104 **Results:**

105 *A complex gene network links the flagellum to holdfast production*

106 We previously described a method called adhesion profiling by which a barcoded transposon
107 library is sequentially passaged in the presence of a cellulose-based substrate. Adhesive mutants
108 become depleted as they colonize the substrate, enriching for mutants with attachment defects in
109 the surrounding broth. By monitoring the mutant population over time, we quantified each gene's
110 contribution to adhesion at the genome scale (33). This initial study identified a set of hyper-
111 adhesive mutants that included genes involved in flagellar assembly, which suggested the

112 presence of a specific signaling pathway linking cues from the flagellum to holdfast production
113 (Fig 1C). We modified our genetic selection to identify a broader range of adhesion-activating
114 mutations by using a defined medium (M2X) in which holdfast production is almost entirely
115 repressed in wild-type *C. crescentus*(35). Under these conditions, dozens of genes displayed
116 adhesion profiles indicative of hyper-adhesion (Fig 1D and Table S1). Though numerous
117 functional categories were represented in this gene set, the overwhelming majority of hyper-
118 adhesive phenotypes were observed in mutants with predicted disruptions to flagellar assembly,
119 chemotaxis or other flagellar processes.

120 We focused on the holdfast phenotype for a mutant (Δ*flgH*) lacking the gene for the
121 flagellar L ring protein(42) growing in M2X medium (Fig 1C). Consistent with previous reports
122 (33, 34), crystal violet (CV) staining of surface attached cells was elevated in Δ*flgH* cultures
123 relative to wild type, and a larger proportion of cells displayed a holdfast when stained with
124 fluorescently labelled wheat germ agglutinin (fWGA, Fig 1C). Mutating genes that code for
125 extracellular components of the *C. crescentus* flagellum was proposed to increase adhesion by
126 rendering cells hyper-sensitive to surface contact(40), but our results indicated that the Δ*flgH*
127 mutant displayed elevated holdfast production when grown in liquid without an activating
128 surface. Though our standard fWGA staining protocol includes brief centrifugation steps, we
129 confirmed that the proportion of holdfast producing cells did not change when centrifugation was
130 omitted and cells were imaged directly from liquid cultures (Fig S1). Additionally, we found that
131 the Δ*flgH* mutant released holdfast polysaccharide directly into spent liquid medium (Fig S1),
132 another hallmark of surface-independent holdfast activation (43). These results are inconsistent
133 with the model that the Δ*flgH* mutant is hyper-sensitive to surface contact. Instead, elevated
134 adhesion in Δ*flgH* results from surface contact-independent increases in both the proportion of

135 cells that assemble a holdfast and the amount of secreted holdfast polysaccharide. We conclude
136 that flagellar mutations act as gain of function activators of holdfast production.

137 To dissect potential pathways linking the flagellum to holdfast production, we constructed
138 a barcoded Tn-*Himar1* library in a Δ*flgH* background and performed a second adhesion profiling
139 experiment with the goal of identifying mutations that suppress the hyper-holdfast phenotype. As
140 in wild type, genes required for holdfast synthesis (*hfs*) were the strongest determinants of
141 adhesion in the Δ*flgH* mutant. In addition, we identified a few dozen genes (called *fss* for flagellar
142 signaling suppressor) that contribute to adhesion specifically in the Δ*flgH* background (Fig 1E,
143 Table S2). While, many of the *fss* genes are uncharacterized, insertions in genes known to promote
144 flagellar rotation, chemotaxis, cell cycle progression and other physiological processes had *fss*
145 phenotypes as well. Both the abundance and functional diversity of the suppressors point to a
146 complex signaling network that links adhesion to flagellar motility.

147

148 *Distinct adhesion patterns in flagellar assembly mutants*

149 Two of the *fss* genes, *motB* and *pleD*, are known to regulate holdfast production under specific
150 conditions. *motB,* which codes for one of the flagellar stator proteins, is required for rapid holdfast
151 synthesis after surface contact in microfluidic chambers(40). *pleD,* which codes for a diguanylate
152 cyclase that regulates morphogenesis during the swarmer-to-stalked transition(44), contributes
153 to increased holdfast production in a flagellar hook mutant background through a process
154 independent of surface contact(34). Previous examinations of these two genes have produced
155 conflicting models for how surface contact, flagellar assembly and filament rotation modulate
156 holdfast production. Identifying mutations in both *pleD* and *motB* as suppressors of Δ*flgH*
157 suggested that we could clarify the signaling pathway that links flagellar perturbations to holdfast
158 production.

159 We used CV staining to examine how disrupting *pleD* and *motB* affects adhesion to
160 polystyrene in various flagellar mutant backgrounds. Disrupting the early stages of flagellar
161 assembly by deleting the class II genes *fliF* or *fliM* led to a hyper-adhesive phenotype that was
162 strongly suppressed by deletion of *pleD* but that was not affected by deletion of *motB.* In contrast,
163 when holdfast production was stimulated by deletion of the class III gene *flgH* or disruption of
164 flagellin secretion (Δ*flmA*)(45), the hyper-adhesive phenotype was suppressed by introducing
165 either a *pleD* or a *motB* deletion (Fig 2A). Thus, flagellar mutants stimulate adhesion through
166 different mechanisms. Mutants that disrupt the early stages of assembly activate holdfast
167 production through *pleD*, while mutants in which assembly is stalled at later stages stimulate
168 adhesion through both *pleD* and *motB.*
169
170 *Two pathways modulate holdfast production downstream of the flagellum*
171 The distinct suppression patterns in *pleD* and *motB* mutants indicated that multiple pathways
172 function downstream of the flagellum to influence adhesion. Indeed, combining the Δ*pleD* and
173 Δ*motB* mutations reduced CV staining to near un-detectable levels in both the wild-type and Δ*flgH*
174 backgrounds, supporting the model that *pleD* and *motB* control attachment through distinct
175 mechanisms (Fig 2B, Fig S2A). The severe adhesion defect observed for the Δ*pleD* Δ*motB* double
176 mutant demonstrates that the *pleD*- and *motB*-dependent pathways do not operate exclusively in
177 the context of flagellar mutants. Either the *pleD* or *motB* pathway must be intact for *C. crescentus*
178 to colonize surfaces.
179 We quantified holdfast production by staining cells from a representative panel of mutants
180 with fWGA. The proportion of cells displaying a holdfast was elevated in both early (Δ*fliF*) and late
181 (Δ*flgH*) flagellar assembly mutants, and the suppression patterns seen by CV staining were
182 recapitulated with fWGA staining. Holdfast production was elevated to similar levels in Δ*fliF* and

183 Δ*fliF* Δ*motB* but nearly eliminated in Δ*fliF* Δ*pleD.* Introducing either the Δ*pleD* or the Δ*motB*
184 mutations reduced holdfast production in a Δ*flgH* background, and holdfast production was nearly
185 undetectable in Δ*pleD* Δ*motB* and Δ*flgH* Δ*pleD* Δ*motB* cultures (Fig 2C and Table S3). We did
186 identify modest discrepancies between the holdfast production and polystyrene colonization
187 measurements. Although surface attachment was indistinguishable from wild type in Δ*motB*
188 cultures, holdfast production in this mutant was elevated. This agrees with previous
189 measurements indicating that non-motile strains display holdfast-independent surface
190 colonization defects (33, 34). Separately, CV staining was higher in Δ*flgH* cultures than in Δ*fliF*
191 cultures, but the proportion of holdfast producing cells was higher in the Δ*fliF* mutant. Because
192 both strains are non-motile, the discrepancy is likely due to modulation of additional holdfast-
193 independent colonization factors such as type IV pilus dynamics(33, 46).

194 Finally, we examined expression of the *holdfast inhibitor A* (*hfiA*) gene, a key regulator that
195 inhibits adhesion by targeting a glycosyltransferase in the holdfast biosynthesis pathway (Fig
196 2D)(35). Increased holdfast production in the Δ*flgH* and Δ*motB* backgrounds is accompanied by a
197 decrease in P_{hifA}-*lacZ* reporter activity, but elevated holdfast production in the Δ*fliF* mutant occurs
198 without a reduction in *hfiA* transcription (Fig 2D and Table S3). Introducing either the Δ*motB* or
199 Δ*pleD* mutations into the Δ*flgH* background restored P_{hifA} activity to wild-type levels. These
200 measurements show that *pleD* is required for downregulation of *hfiA* in the Δ*flgH* background, but
201 do not clarify the role of *motB.* It remains unclear how the Δ*motB* mutation attenuates *hfiA*
202 promoter activity in the wild-type background but restores normal expression in a Δ*flgH* mutant.
203 Transcription from the *hfiA* promoter was elevated in the Δ*pleD* Δ*motB,* the Δ*flgH* Δ*pleD* Δ*motB*
204 and the Δ*fliF* Δ*pleD* mutants, indicating that activation of *hfiA* expression contributes to the severe
205 holdfast production defect in these three strains.

206 Transcription of *hfiA* is finely tuned by a complex hierarchy of transcription factors such
207 that small changes in expression have significant impacts on holdfast production (33, 35, 37). The
208 three non-adhesive mutants analyzed in Figure 2 display robust increases in *hfiA* expression, and
209 the Δ*fliF* mutant shows a striking increase in holdfast production that clearly occurs
210 independently of *hfiA* regulation. However, P_{hifA}-*lacZ* activity differences for other key strains are
211 modest and do not correlate perfectly with direct measurements of holdfast production. While
212 cell-cycle control and post-transcriptional processes can be masked in bulk reporter
213 measurements, the expression level changes in flagellar signaling mutants are less pronounced
214 than for regulatory systems that target *hfiA* directly (35, 37). A significant portion of adhesion
215 control exerted by the flagellum likely occurs independent of *hfiA* regulation.
216
217 *Parsing regulatory networks with epistasis analysis*
218 The distinct activation profiles observed in early and late flagellar assembly mutants were used to
219 assign *fss* genes to either the *pleD*- or *motB*-dependent signaling pathways. We predicted that *pleD*
220 and other genes involved in stalked cell morphogenesis make up a "developmental" signaling
221 pathway and that genes associated with stator activity make up a second, "mechanical" pathway.
222 This model predicts that developmental pathway mutants should block holdfast stimulation in
223 both early and late flagellar assembly mutant backgrounds, while mechanical pathway mutants
224 should suppress hyper-adhesion specifically in late assembly mutants. Two additional *fss* genes,
225 *shkA* and *dgcB,* were used to test these predictions. *shkA* encodes a histidine kinase that regulates
226 stalk development(47), and *dgcB* codes for a diguanylate cyclase that physically associates with
227 stator subcomplexes(40). Deleting *shkA* suppressed the hyper-adhesive effects of both the Δ*fliF*
228 (early) and the Δ*flgH* (late) mutations, while deleting *dgcB* suppressed adhesion in the Δ*flgH*
229 background but had no effect in the Δ*fliF* background (Fig 3A). Furthermore, adhesion was nearly

230 eliminated when the Δ*shkA* mutation was introduced into the Δ*motB* or Δ*dgcB* backgrounds (Fig
231 S2), confirming that *shkA* signals through a mechanism distinct from that of mechanical pathway
232 genes. These results provide further support for a model in which both a developmental pathway
233 associated with stalked cell morphogenesis and a mechanical pathway associated with stator
234 activity function downstream of the flagellum to activate adhesion.

235 We also used epistasis to place two uncharacterized genes identified as Δ*flgH* suppressors
236 into the mechanical signaling pathway. *fssA* (*CC_1064*; *CCNA_01117*) encodes a protein with a
237 Sec/SP1 secretion signal and no predicted functional domains. *fssB* (*CC_2058*; *CCNA_02137*)
238 encodes a protein with a Sec/SP1 secretion signal and a predicted tetratricopeptide repeat (TPR)
239 domain. Deleting either *fssA* or *fssB* did not affect adhesion in the wild-type or Δ*fliF* backgrounds
240 but suppressed the hyper-adhesive phenotype in Δ*flgH* (Fig 3A), providing evidence that *fssA* and
241 *fssB* contribute to holdfast stimulation through the stator-dependent, mechanical pathway.

242

243 *New motility factors contribute to mechanical activation*

244 To understand how *fssA* and *fssB* regulate holdfast synthesis, we examined the motility
245 phenotypes of Δ*fssA* and Δ*fssB* deletions. Both mutants were severely impaired in their ability to
246 spread through soft agar. When a flagellin allele (*fljK*^{T103C}) coding for an FljK protein that can be
247 stained with maleimide-conjugated dyes(34) was introduced, flagellar filaments were observed in
248 both Δ*fssA* and Δ*fssB* cells. Thus, the motility phenotypes in these mutants are not caused by
249 disruptions to flagellar assembly. Examination of individual cells in liquid broth revealed that
250 Δ*fssB* cells were non-motile, while some Δ*fssA* cells retained the ability to swim (Fig 3C). Thus, the
251 Δ*fssB* mutant displays a paralyzed flagellum phenotype analogous to a Δ*motB* mutant, but the
252 motility phenotype in Δ*fssA* is specific to soft agar.

253 Over the course of our studies, we observed that the Δ*fssA* mutant had a propensity to
254 begin spreading through soft-agar after prolonged incubation on plates (Fig 4A). Colonies
255 migrated from the inoculation site in an anisotropic manner, suggesting that second-site
256 suppressors of the motility defect had emerged. Indeed, single colonies isolated from motile Δ*fssA*
257 flares were indistinguishable from wild-type when re-inoculated into soft-agar. Fourteen of these
258 motile suppressors were analyzed by whole genome sequencing to identify the causative
259 mutations. Each isolate harbored a missense mutation in one of the stator genes. Three contained
260 a mutation in *motA,* and eleven contained a mutation in *motB.* Nine of the eleven *motB* mutations
261 disrupt the same residue, serine 52, and six produce the same allele, $motB^{S52C}$ (Fig S3).

262 We used a cryoelectron microscopy reconstruction of the MotAB stator from
263 *Campylobacter jejuni*(48) to predict the structure of the *C. crescentus* stator complex. The resulting
264 homology model contains a characteristic transmembrane channel composed of five MotA
265 subunits that is capped at its periplasmic face by two MotB protomers(48, 49). When Δ*fssA*
266 suppressing mutations were mapped onto this model they displayed a clear bias toward residues
267 on the periplasmic face of the complex (Fig 4B), with the *motB* mutations all disrupting a region
268 known as the plug. Deleting the plug allows ion translocation through the stators in the absence of
269 productive engagement with a rotor(50), and missense mutations in the plug have been shown to
270 support motility under nonpermissive conditions through gain of function activation of the
271 motor(51).

272 The ability of plug mutations to suppress the Δ*fssA* motility defect indicates that Δ*fssA* and
273 Δ*fssB* display related motility phenotypes. Δ*fssB* produces an inactive flagellar motor that cannot
274 turn a filament (Fig 3C), while Δ*fssA* assembles a modestly defective motor that supports full
275 motility in soft-agar only when the stators are activated by mutations predicted to increase ion
276 translocation (Fig 4). A Δ*fssA* Δ*fssB* double mutant did not spread through soft-agar even after

277 prolonged incubation, confirming that the lack of motor rotation in Δ*fssB* is epistatic to the partial
278 defect in Δ*fssA* (Fig S3). Furthermore, our data indicate that *fssA* and *fssB* support flagellar
279 signaling by the same the mechanism, as the Δ*fssA* and Δ*fssB* mutations did suppress Δ*flgH* hyper-
280 adhesion in an additive manner (Fig S3). We conclude that *fssA* and *fssB* are required for proper
281 stator activity in *C. crescentus.* We propose that mutating either gene disrupts both the stator's
282 ability to promote motility and its capacity to transduce mechanical signals.
283
284 *Separate mechanisms for activating c-di-GMP production*
285 Though the developmental and mechanical pathways can be separated genetically, they ultimately
286 converge to modulate holdfast production. Each pathway includes a diguanylate cyclase predicted
287 to synthesize bis-(3'-5')-cyclic diguanosine monophosphate (c-di-GMP), a second messenger that
288 promotes surface-associated behaviors in bacteria(52). In *C. crescentus,* c-di-GMP binds numerous
289 downstream effectors to activate stalk assembly(53), cell cycle progression(54, 55) and holdfast
290 synthesis (40, 56). To test the role of c-di-GMP synthesis in linking cues from the flagellum to
291 holdfast production, we examined catalytically inactive alleles of *pleD* and *dgcB.* In contrast to
292 wild-type alleles, $pleD^{E370Q}$(57) and $dgcB^{E261Q}$(40) failed to restore hyper-adhesion in the Δ*flgH*
293 Δ*pleD* and Δ*flgH* Δ*dgcB* backgrounds, respectively, confirming that c-di-GMP synthesis by these
294 enzymes is required to support flagellar signaling through both the mechanical and
295 developmental pathways (Fig 5A).
296 We examined mechanisms by which the diguanylate cyclase activities of PleD and DgcB are
297 activated during flagellar signaling. PleD contains a receiver domain at its N-terminus that
298 includes a canonical aspartyl phosphorylation site(57, 58). Introducing the non-phosphrylatable
299 $pleD^{D53N}$ allele failed to restore hyper-adhesion in the Δ*flgH* Δ*pleD* background (Fig 5A). We
300 conclude that phosphorylation of the PleD receiver domain is required for flagellar perturbations

301 to stimulate holdfast production through the developmental pathway. Proton translocation by
302 MotAB stators is used to generate torque for flagellar filament rotation. A *motB* allele (*motB*^{D33N})
303 that prevents proton flux through the stator(40, 59) does not support flagellar signaling in the
304 Δ*flgH* background (Fig 5A). We conclude that proton translocation through MotB is required for
305 flagellar perturbations to stimulate holdfast production via the mechanical pathway.

306 Our data indicate that active proton translocation is required for mechanical stimulation.
307 This model provides a possible explanation for the disparate suppression patterns we observed in
308 early and late flagellar assembly mutants. We predicted that the mechanical pathway is inactive in
309 early flagellar mutants because stator subunits cannot engage with the motor when rotor
310 assembly is incomplete. Indeed, Δ*fliF* was epistatic to Δ*flgH* with respect to suppression by Δ*pleD*
311 and Δ*motB* (Fig 5B). Adhesion in the Δ*fliF* Δ*flgH* mutant was eliminated when *pleD* was deleted but
312 remained unchanged when the Δ*motB* mutation was introduced, supporting the model that inner
313 membrane rotor assembly is required for activation of the mechanical pathway.

314

315 **Discussion:**

316 Many bacteria alter their behavior after contact with exogenous surfaces, and flagellar motility is a
317 key regulatory determinant of these responses(38, 60–63). However, efforts to dissect contact-
318 dependent signaling pathways have been confounded by contributions from multiple
319 mechanosensors(62, 64), a reliance on non-canonical signaling machinery(9, 40) and the
320 prevalence of transcription-independent responses(7, 65). In this study, we leveraged the hyper-
321 adhesive phenotype induced upon mutation of flagellar assembly genes to dissect the genetic basis
322 for adhesion control by the flagellum in *C. crescentus*. We used a high-throughput phenotyping
323 approach to identify mutations that stimulate adhesion and to classify a large group of genes
324 called *flagellar signaling suppressors* (*fss*) that contribute to increased holdfast production when

325 flagellar assembly is disrupted. The results have clarified important features of how the *C.*
326 *crescentus* flagellum regulates adhesion and provided a framework for disentangling signaling
327 networks that control bacterial behavior.

328 Two genes identified in the *fss* screen, *pleD* and *motB,* have been previously shown to link
329 flagellar function to adhesion, but conflicting models were proposed for how these genes regulate
330 holdfast production(34, 40). We showed that *pleD* and *motB* participate in genetically distinct
331 pathways for activating adhesion. *pleD* and its downstream effector *shkA* contribute to increased
332 holdfast production when any stage of flagellar assembly is disrupted. *motB,* the gene for its
333 associated diguanylate cyclase, *dgcB*, and two previously uncharacterized motility genes
334 contribute to adhesion specifically in late flagellar mutants that retain the ability to assemble
335 inner membrane rotors. We conclude that a mechanical pathway and a developmental pathway
336 operate in parallel to link flagellar function to holdfast production.

337 Strains harboring deletions (Δ*motB,* Δ*fssA,* or Δ*fssB*) or mutant alleles (*motB*^{D33N}) that
338 disrupt motility without affecting filament assembly cannot support activation of the mechanical
339 pathway (Figs 2A, 3A and 5A). Additionally, early flagellar assembly mutants display epistatic
340 effects on late assembly mutants by eliminating *motB*'s involvement in stimulating adhesion (Fig
341 5B). These results suggest that blocking inner membrane rotor (MS- and C-ring) assembly
342 subverts the mechanical pathway by preventing stator engagement and help to explain the range
343 of behavioral effects often observed in flagellar assembly mutants(5, 40, 66). We conclude that
344 intact motors capable of generating torque are required for mechanical activation of the *C.*
345 *cresecentus* flagellum. Increased load on rotating filaments leads to the recruitment of additional
346 stators to the motor in enteric bacteria(67, 68), and a similar resistance sensing mechanism likely
347 supports tactile sensing in *C. crescentus*. Mutants in mechanical pathway genes such as *fssA* and

348 *fssB* should prove useful in describing the structural basis for how such changes in load are sensed
349 by the flagellar motor.

350 Key features of the mechanical pathway mirror the tactile sensing event described by Hug
351 and colleagues(40), but certain conclusions must be reevaluated in light of our results. We showed
352 that late flagellar mutants display increased holdfast production in M2X liquid medium (Fig 2C
353 and Fig S1) in the absence of a surface and under nutrient conditions for which tactile sensing
354 does not normally occur(34). We conclude that mutants lacking the outer parts of the flagellum do
355 not show a hyper-sensitive surface response. Instead, we infer that the motor responds to the
356 absence of a filament as it would to an obstructed filament by activating stator-dependent
357 signaling ectopically. Consistent with this interpretation, preventing stators from productively
358 engaging with the rotor, either by disrupting proteins required for stator function (Figs 2A and
359 3A) or by mutating early flagellar genes that code for rotor components, blocks mechanical
360 signaling in late assembly mutants (Fig 5B). This explains the perplexing epistasis of inner parts of
361 the flagellum over outer parts(69) and supports established models for tactile sensing through
362 increased load on the filament(60) rather than the motor acting as a tetherless sensor(40). More
363 broadly, the disparate phenotypes identified here for stator, rotor and hook-basal body mutants
364 reflect an emerging pattern seen in other organisms and argue that signal bifurcation by the
365 flagellum is a conserved feature throughout bacteria(70, 71).

366 The identification of a second, developmental pathway downstream of the flagellum is
367 consistent with previous studies showing that late flagellar assembly mutants display contact-
368 independent increases in holdfast production(33, 34). In fact, disrupting flagellar assembly at any
369 stage stimulates adhesion (Fig 2A), and our analysis of this process highlights an overlooked role
370 for the flagellum in controlling the *C. crescentus* developmental program. We explicitly
371 characterized *pleD* and *shkA*, but other developmental regulators identified in the *fss* screen (*shpA*,

372 *tacA*(47), *spmX*(72), *spmY*(73), *zitP*, *cpaM*(74), *sciP*(75), *rpoN*(76)) likely also act downstream of
373 both early and late flagellar mutants to stimulate adhesion. Most of these genes influence flagellar
374 assembly either directly or by altering cell cycle progression. For instance, *pleD* promotes flagellar
375 disassembly by stimulating proteolytic turnover of the MS-ring protein FliF (77), but our results
376 indicate that PleD is also stimulated through phosphorylation at D53 when flagellar assembly is
377 disrupted (Fig 4A). Thus, cell cycle regulators that control flagellar assembly simultaneously act
378 downstream of the flagellum in regulating holdfast production. This duality raises the intriguing
379 possibility that specific environmental cues activate flagellar disassembly as part of a positive
380 feedback loop that reinforces the commitment to differentiate into a stalked cell.

381 The developmental and mechanical pathways we identified each require a distinct
382 diguanylate cyclase, suggesting that flagellar signaling converges to stimulate adhesion by
383 modulating c-di-GMP levels (Fig 4C). Signaling through the mechanical pathway requires stator
384 subunits that can productively engage with the rotor, and we propose that increased load on the
385 flagellar filament induces conformational changes in the motor that activate the stator-associated
386 diguanylate cyclase DgcB. This mechanism differs from contact-dependent activation of c-di-GMP
387 synthesis by SadC in *Pseudomonas aeruginosa*, which requires disengagement of the MotCD
388 stator(78). *P. aeruginosa* uses a MotAB stator system for swimming in liquid and a second, MotCD
389 stator for swarming on surfaces(79). Thus, the signaling competency of engaged stators in *C.*
390 *crescentus* could be an intrinsic feature of single-stator systems. Separately, c-di-GMP synthesis by
391 PleD is part of a multi-tiered system controlling the master cell-cycle regulator CtrA in *C.*
392 *crescentus*(53, 80), and we provided evidence that the status of flagellar assembly feeds into this
393 developmental program by regulating PleD phosphorylation (Fig 5A). Whether the flagellum
394 controls PleD phosphorylation through the DivJ-PleC kinase-phosphatase pair(57) or through a

395 separate phosphorelay will require additional dissection of how *fss* genes link flagellar assembly
396 to cell cycle progression.

397 Despite the apparent convergence of flagellar signaling on two diguanylate cyclases, *pleD*-
398 and *dgcB* stimulate holdfast production by different mechanisms. When the mechanical pathway
399 is bypassed by disrupting early stages of flagellar assembly, *shkA* and *pleD* are required for
400 holdfast production, but *dgcB* is dispensable (Figs 2A and 3A). ShkA is a histidine kinase that is
401 stimulated by c-di-GMP(81). It initiates a phosphotransfer that activates the transcriptional co-
402 activator TacA, upregulating dozens of genes required for stalk biogenesis(47). A requirement for
403 both *pleD* and *shkA* in the developmental pathway indicates that *pleD* controls holdfast production
404 specifically through the *tacA* transcriptional program. In contrast, the *dgcB*-dependent c-di-GMP
405 pool has been shown to act through direct activation of holdfast synthesis enzymes (40). Thus,
406 PleD and DgcB likely act on different timescales, and we favor a model in which the sequential
407 accumulation of c-di-GMP drives the transition to permanent attachment. In this scenario,
408 increased load on the flagellar filament would activate DgcB, producing a transient burst of c-di-
409 GMP that immediately stimulates holdfast production. Persistent filament obstruction would
410 increase c-di-GMP levels sufficiently to destabilize the motor, leading to flagellar disassembly,
411 activation of sustained c-di-GMP synthesis by PleD and the onset of stalked cell development (Fig
412 5C).

413 Using an unbiased screen to identify flagellar signaling genes has allowed us to propose a
414 unified model for the mechanism by which the flagellum regulates holdfast production in *C.*
415 *crescentus*. Intact flagellar motors respond to assembly defects in their associated filaments (Figs
416 2A and 5B), but perturbing the flagellum also influences the timing of holdfast production by
417 altering cell cycle signaling (34)(Figs 2A and 5A). Candidate approaches specifically targeting
418 developmental or tactile sensing phenomena have not accounted for presence of multiple

419 pathways downstream of the flagellum. Though two pathways can be distinguished genetically in
420 flagellar mutants, overlap between developmental, mechanical and other signaling pathways
421 during actual surface encounters has likely confounded interpretations of how the flagellum
422 regulates holdfast production. The complexity of these circuits underscores how bacterial
423 behavior is not controlled by linear signaling pathways. Flagellar cues represent only a subset of
424 the stimuli known to influence adhesion. Nutrient availability, redox homeostasis, chemotaxis and
425 T4P dynamics all influence whether *C. crescentus* produces a holdfast. Disentangling how diverse
426 signaling networks converge to regulate holdfast production has the power to illuminate how
427 environmental information is integrated to control behavior.
428
429 **Materials and Methods:**
430 *Bacterial growth and genetic manipulation*
431 Strains and plasmids used in this study are listed in Tables S4 and S5. Standard polymerase chain
432 reaction (PCR) and Gibson assembly(82) methods were used for developing plasmid constructs.
433 Strains, plasmids, primer sequences and details of construction are available upon request. *E. coli*
434 cultures were grown in LB medium at 37°C supplemented with 1.5% (w/v) agar and 50 μg/mL
435 kanamycin when necessary. Unless otherwise noted, *C. crescentus* cultures were grown at 30°C in
436 PYE medium supplemented with 1.5% (w/v) agar, 3% (w/v) sucrose and 25 μg/mL kanamycin
437 when necessary or in M2 defined medium supplemented with 0.15% (w/v) xylose (83). Plasmids
438 were introduced into *C. crescentus* by electroporation. Unmarked deletions were constructed
439 using *sacB*-based counterselection in sucrose as described previously(33).
440
441 *Genetic complementation of mutants*

442 Mutants were complemented by genomic integration of the appropriate gene as a single copy at a
443 neutral site (*xylX*) and under the gene's native promoter. Specifically, predicted open reading
444 frames were fused to their predicted promoter sequences and inserted into the NdeI/SacI site of
445 pMT585 (pXGFPC-2)(84). Each promoter-gene cassette was inserted in reverse orientation to
446 allow for transcription in the opposite direction relative to the *xylX* promoter upstream of the
447 cloning site. Surface attachment and motility assays used to evaluate complementation are
448 described below (Fig S4).
449
450 *Tn-Himar mutant library construction and mapping*
451 Construction and mapping of the two barcoded transposon libraries was performed based on the
452 procedure developed by Wetmore et al. as described previously(33, 85). Cells from 25 mL cultures
453 of the APA_752 barcoded transposon pool that had been grown to mid-log phase in LB
454 supplemented with kanamycin and 300 μM diaminopimelic acid (DAP) and 25mL of either the *C.*
455 *crescentus* CB15 wild-type or Δ*flgH* strain that had been grown to mid-log phase in PYE were
456 collected by centrifugation, washed twice with PYE containing 300 μM DAP, mixed and spotted
457 together on a PYE agar plate containing 300 μM DAP. After incubating the plate overnight at room
458 temperature, the cells were scraped from the plate, resuspended in PYE medium, spread onto 20,
459 150mm PYE agar plates containing kanamycin and incubated at 30°C for three days. Colonies from
460 each plate were scraped into PYE medium and used to inoculate a 25mL PYE culture containing 5
461 μg/mL kanamycin. The culture was grown for three doublings, glycerol was added to 20%, and 1
462 mL aliquots were frozen at -80°C.
463 Library mapping was performed as described (85). Briefly, genomic DNA was isolated from
464 three 1mL aliquots of each library. The DNA was sheared and ~300bp fragments were selected
465 before end repair. A Y-adapter (Mod2_TS_Univ, Mod2_TruSeq) was ligated and used as a template

466 for transposon junction amplification with the primers Nspacer_BarSeq_pHIMAR and either
467 P7_mod_TS_index1 or P7_mod_TS_index2. 150-bp single end reads were collected on an Illumina
468 HiSeq 2500 in rapid run mode, and the genomic insertion positions were mapped and correlated
469 to a unique barcode using BLAT(86) and MapTnSeq.pl to generate a mapping file with
470 DesignRandomPool.pl. All code is available at https://bitbucket.org/berkeleylab/feba/. Features
471 of the barcoded transposon libraries can be found in Table S6.
472
473 *Adhesion profiling of barcoded Tn-Himar mutant libraries*
474 Adhesion profiling was performed as in Hershey et al. (33) with slight modifications. Cells from
475 1mL aliquots of each barcoded transposon library were collected by centrifugation, resuspended
476 in 1mL of M2X medium, and 300 µL was inoculated into a well of a 12-well microtiter plate
477 containing 1.5mL M2X medium with 6-8 ~1 x 1 cm layers of cheesecloth. Microtiter plates
478 containing selections were grown for 24hr at 30°C with shaking at 155rpm after which 150µL of
479 the culture was passaged by inoculating into a well with 1.65mL fresh M2X containing
480 cheesecloth. Cells from an additional 500µL of depleted medium were harvested by centrifugation
481 and stored at -20°C for BarSeq analysis. Each passaging experiment was performed in triplicate,
482 and passaging was performed sequentially for a total of five rounds of selection. Identical cultures
483 grown in a plate without cheesecloth were used as a nonselective reference condition.
484 Cell pellets were used as PCR templates to amplify the barcodes in each sample using
485 indexed primers(85). Amplified products were purified and pooled for multiplexed sequencing.
486 50bp single end reads were collected on an Illumina HiSeq4000. MultiCodes.pl, combineBarSeq.pl
487 and FEBA.R were used to determine fitness by comparing the $\log_2$ ratios of barcode counts in each
488 sample over the counts from a nonselective growth in M2X without cheesecloth. To evaluate
489 mutant phenotypes in each screen, the replicates were used to calculate a mean fitness score for

490 each gene after each passage. Mean fitness was summed across passages for each gene and ranked
491 by either the lowest (WT background) or highest (Δ*flgH* background) summed fitness score.
492
493 *Surface attachment measurement by crystal violet (CV) staining*
494 Overnight *C. crescentus* cultures grown in PYE were diluted to an OD_{660} of 0.5 with PYE, and 1.5 µL
495 from each diluted starter culture was inoculated into the wells of a 48-well microtiter plate
496 containing 450 µL M2X medium. The number of replicates for each experiment ranged from 5-8
497 and is indicated in the relevant figure legend. Plates were grown at 30°C with shaking at 155rpm
498 for 17 hours after which the cultures were discarded, and the wells were washed thoroughly
499 under a stream of tap water. Attached cells were stained by adding 500 µL of an aqueous solution
500 containing 0.01% (w/v) crystal violet to each well and shaking the plates for 5 min. Excess dye
501 was discarded, the wells were again washed under a stream of tap water and the remaining dye
502 was dissolved by adding 500 µL of ethanol to each well. Staining was quantified by reading
503 absorbance at 575nm using a Tecan Spark microplate reader. Each reading was corrected by
504 subtracting the absorbance value for an uninoculated medium blank, the mean of the biological
505 replicates for each strain was calculated and normalized to the mean value measured for the wild
506 type background. To minimize day-to-day variation in the absolute CV staining values, each figure
507 panel shows an internally controlled experiment with all measurements taken from the same
508 plate on the same day. The collection of strains shown in each figure was assayed together on at
509 least four independent days and a representative dataset is shown.
510
511 *Holdfast staining with fluorescent wheat germ agglutinin (fWGA)*
512 2mL of M2X medium was inoculated to achieve a starting OD_{660} of 0.001 using saturated starter
513 cultures grown in PYE. After growing to an OD_{660} of 0.07-0.1, 400 µL of each culture was added to

514 a fresh 1.5mL ependorf tube containing 1 μL of a 2mg/mL solution of WGA conjugated with
515 Alexa594. After a 5min incubation at room temperature in the dark, cells were harvested at 6k x g,
516 washed with distilled water, and resuspended in the residual liquid after centrifugation. 1 μL was
517 spotted onto a glass slide and a cover slip was placed on top. Imaging was performed with a Leica
518 DM5000 microscope equipped with an HCX PL APO63X/1.4-numerical-aperture Ph3 objective. A
519 red fluorescent protein filter (Chroma set 41043) was used to visualize WGA foci. Cells with a
520 holdfast were counted manually on five separate days. A minimum of 95 cells were counted for
521 each biological replicate.

522 For direct staining of liquid cultures without centrifugation, cells were grown as described
523 above. 400 μL was removed and imaged using the standard protocol described above, and 0.8 μL
524 from a 2mg/mL fWGA solution was added directly to the remaining culture. Cultures were shaken
525 with the dye for 5 min in the dark after which 1.5 μL was spotted on a microscope slide, covered
526 and imaged immediately as described above.

527

528 *Analysis of holdfast polysaccharide in spent medium*

529 Holdfast release was analyzed as described previously(43). 10mL cultures grown for 24 hours in
530 M2X were centrifuged at 7k x g for 10 min. 2mL of supernatant (spent medium) was moved to a
531 fresh tube, 3mL of 100% ethanol was added, and the mixture was incubated overnight at 4°C.
532 Precipitate was isolated by centrifugation for 1hr at 18,000 x g and suspended in 50 μL TU buffer
533 (10mM Tris-HCl pH 8.2, 4M urea). 2-fold serial dilutions were prepared, and 3 μL of each dilution
534 was spotted on nitrocellulose to absorb for 20 min. The membrane was then blocked overnight
535 with 5% bovine serum albumin (BSA) dissolved in TBST buffer (20mM Tris-HCl pH 8.0, 137mM
536 NaCl, 2.7mM KCl, 0.1% Tween 20) followed by a 1hr incubation with 5% BSA in TBST containing

537 1.5 ug/mL fWGA. The membrane was washed with TBST and imaged with a BioRad ChemiDoc
538 imager using the Alexa Fluor 647 setting.
539
540 *Soft-agar motility assay*
541 Overnight cultures grown in PYE were diluted to OD_{660} = 0.5, and 1.5 µL was pipetted into a PYE
542 plate containing 0.3% agar. Plates were sealed with parafilm, incubated for 72 hours at 30°C and
543 photographed.
544
545 *Flagellar filament staining*
546 2mL of PYE medium was inoculated to a starting OD_{660} = 0.05 using saturated overnight starter
547 cultures and grown at 30°C to mid-log phase (OD_{660} = 0.3 – 0.4). 500 µL of each culture was mixed
548 with 0.5 µL of a 2mg/mL solution of Alexa488-maleimide in DMSO and incubated for 10min in the
549 dark. Cells were harvested by centrifuging at 6k x g for 1.5 min, washed with 500 µL PYE, re-
550 centrifuged and suspended in 500 µL PYE. 1 µL of the stained cell suspension was spotted on a pad
551 of PYE solidified with 1% agarose. Imaging was performed as above but with the use of green
552 fluorescent protein filter (Chroma set 41017) for flagellin visualization. Note that Alexa-488
553 maleimide cross-reacts with the holdfast.
554
555 *Microscopic analysis of swimming behavior*
556 2mL of PYE was inoculated to OD_{660} = 0.1 with saturated overnight starters and grown at 30°C to
557 OD_{660} = 0.4 – 0.5. A 2.69% (w/v) solution of 2.0 µm polystyrene spacer beads (Polysciences) was
558 diluted 1000-fold in 1mL PYE. Equal volumes of liquid culture and diluted spacer beads were
559 mixed and spotted on a slide. Dark field images were collected at 100ms intervals for 30s using a
560 Leica 40X PH2 objective. Maximum projections from each time series are presented.

561

562 *Mapping of suppressing mutations in Δ*fssA

563 To isolate motile suppressors, 1.5 µL from a saturated Δ*fssA* culture grown in PYE was spotted into
564 PYE plates containing 0.3% agar. Plates were sealed and incubated for 96 hours at 30°C. Cells from
565 the leading edge of spreading flares (Fig 4A) were streaked onto a standard PYE plate, and the
566 plates were incubated at 30°C for 72 hours. A single colony was inoculated into PYE broth and
567 grown to saturation. To avoid isolating siblings, only one suppressor was isolated from each initial
568 soft-agar spotting. Genomic DNA from fourteen suppressors as well as the original Δ*fssA* parent
569 background was isolated as described above. Libraries were prepared based on the Illumina
570 Nextera protocol and single end reads were collected using the NextSeq 550 platform at the
571 Microbial Genome Sequencing Center (MiGS, Pittsburgh, USA). Mutations were identified using
572 breseq(87) with the *C. crescentus* NA1000 as a reference genome (GenBank CP001340).

573

574 *Homology modelling of CcMotAB*

575 To develop a structural model of the *C. crescentus* stator, we used the MotA and MotB protein
576 sequences (accessions CCNA_00787 & CCNA_01644) to search a protein structure fold library
577 using the HHpred/HHSearch package for homology detection (88) within the Phyre2 pipeline(89).
578 For *C. crescentus* MotB, this approach yielded high confidence (>99%) structural models of the N-
579 and C-terminal halves of the protein that aligned to multiple published MotB structures, including
580 the N-terminus of *C. jejuni* MotB (PDB ID: 6YKM). The *C. crescentus* MotA model aligned to the
581 entire length of *Campylobacter jejuni* MotA (PDB ID: 6YKM) with high confidence (100%). The
582 coordinates of the *Cc*MotA and N-terminal *Cc*MotB homology models were used to build a 5:2
583 MotA:MotB complex by aligning to the 6YKM *C. jejuni* MotAB model.

584

585 *β-galactosidase assay*

586 Strains carrying a P_{hfiA}-*lacZ* transcriptional reporter (35) were inoculated from colonies on PYE-
587 agar plates into 2 ml M2X medium and grown shaking at 200 RPM overnight at 30°C. Overnight
588 cultures were diluted in 2 ml of fresh M2X to an OD_{660} of 0.05 and grown for approximately 6
589 hours to early exponential phase. These cultures were then diluted again into 2 ml fresh M2X to an
590 OD_{660} of 0.001 and grown for 17 hours to a final OD660nm of 0.1. *β* -galactosidase activity was
591 then was measured colorimetrically as previously described(35). Briefly, 0.15 ml of cells were
592 permeabilized by vortexing with 50 ul of chloroform and 50 ul of PYE broth as an emulsifier. 600
593 ul of Z-buffer (60 mM Na_2HPO_4, 40 mM NaH_2PO_4, 10 mM KCl, 1 mM $MgSO_4$) was added, followed
594 by 200 ul ONPG in 0.1 M KPO_4. After 5 minutes at room temperature, reactions were quenched
595 with 1 ml of 1 M Na_2CO_3 and absorbance at 420nm was used to calculate *β* -galactosidase activity.

596

597 *Data availability*

598 Sequence data have been deposited in the NCBI Sequence Read Archive (SRA) with the following
599 project accessions. For wild-type *C. crescentus,* PRJNA640825 contains the sequence data used to
600 map the barcoded TnHimar library, and PRJNA640525 contains barcoded amplicon sequences
601 collected after passaging in cheesecloth. For the Δ*flgH* mutant, PRJNA640725 contains the
602 sequencing data used to map the barcoded TnHimar library, and PRJNA641033 contains barcoded
603 amplicon sequences collected after passaging in cheesecloth. PRJNA672134 contains whole
604 genome sequencing data for the Δ*fssA* parent strain and 14 motile suppressors.

605

606

607 **Acknowledgements**

608 We thank members of the Crosson laboratory, Howard Shuman and Phoebe Rice for helpful
609 discussions. We thank Miette Hennessey for assistance in constructing the *lacZ* reporter strains.
610 This work was supported by NIH grant R01GM087353 to S.C. D.M.H. is supported by the Helen
611 Hay Whitney Foundation.

612

613 **References**

614 1. Zobell CE. 1943. The Effect of Solid Surfaces upon Bacterial Activity. J Bacteriol 46:39–56.

615 2. Donlan RM. 2002. Biofilms: microbial life on surfaces. Emerg Infect Dis 8:881–890.

616 3. Chavez-Dozal A, Gorman C, Erken M, Steinberg PD, McDougald D, Nishiguchi MK. 2013.
617 Predation Response of *Vibrio fischeri* Biofilms to Bacterivorus Protists. Appl Environ
618 Microbiol 79:553–558.

619 4. Berne C, Ellison CK, Ducret A, Brun YV. 2018. Bacterial adhesion at the single-cell level. Nat Rev
620 Microbiol 16:616–627.

621 5. McCarter L, Hilmen M, Silverman M. 1988. Flagellar dynamometer controls swarmer cell
622 differentiation of *V. parahaemolyticus*. Cell 54:345–351.

623 6. Watnick PI, Kolter R. 1999. Steps in the development of a *Vibrio cholerae* El Tor biofilm. Mol
624 Microbiol 34:586–595.

625 7. Levi A, Jenal U. 2006. Holdfast Formation in Motile Swarmer Cells Optimizes Surface
626 Attachment during *Caulobacter crescentus* Development. J Bacteriol 188:5315–5318.

627 8. Mueller RS, McDougald D, Cusumano D, Sodhi N, Kjelleberg S, Azam F, Bartlett DH. 2007. *Vibrio*
628 *cholerae* Strains Possess Multiple Strategies for Abiotic and Biotic Surface Colonization. J
629 Bacteriol 189:5348–5360.

630 9. Petrova OE, Sauer K. 2011. SagS Contributes to the Motile-Sessile Switch and Acts in Concert
631 with BfiSR To Enable *Pseudomonas aeruginosa* Biofilm Formation. J Bacteriol 193:6614–
632 6628.

633 10. Collier J. 2016. Cell cycle control in Alphaproteobacteria. Curr Opin Microbiol 30:107–113.

634 11. Haiko J, Westerlund-Wikström B. 2013. The Role of the Bacterial Flagellum in Adhesion and
635 Virulence. Biology 2:1242–1267.

636 12. Belas R. 2014. Biofilms, flagella, and mechanosensing of surfaces by bacteria. Trends Microbiol
637 22:517–527.

638 13. Aldridge P, Hughes KT. 2002. Regulation of flagellar assembly. Curr Opin Microbiol 5:160–165.

639 14. Ramakrishnan G, Zhao JL, Newton A. 1994. Multiple structural proteins are required for both
640 transcriptional activation and negative autoregulation of *Caulobacter crescentus* flagellar
641 genes. J Bacteriol 176:7587–7600.

642 15. Stephens C, Mohr C, Boyd C, Maddock J, Gober J, Shapiro L. 1997. Identification of the *fliI* and
643 *fliJ* components of the *Caulobacter flagellar* type III protein secretion system. J Bacteriol
644 179:5355–5365.

645 16. Ohta N, Chen L-S, Swanson E, Newton A. 1985. Transcriptional regulation of a periodically
646 controlled flagellar gene operon in *Caulobacter crescentus*. J Mol Biol 186:107–115.

647 17. Jenal U. 2000. Signal transduction mechanisms in *Caulobacter crescentus* development and cell
648 cycle control. FEMS Microbiol Rev 24:177–191.

649 18. Khan S, Dapice M, Reese TS. 1988. Effects of *mot* gene expression on the structure of the
650 flagellar motor. J Mol Biol 202:575–584.

651 19. Blair DF, Berg HC. 1990. The MotA protein of *E. coli* is a proton-conducting component of the
652 flagellar motor. Cell 60:439–449.

653 20. Henrichsen J. 1972. Bacterial surface translocation: a survey and a classification. Bacteriol Rev
654 36:478–503.

655 21. Schneider WR, Doetsch RN. 1974. Effect of Viscosity on Bacterial Motility. J Bacteriol 117:696–
656 701.

657 22. Berg HC, Tedesco PM. 1975. Transient response to chemotactic stimuli in *Escherichia coli*. Proc
658 Natl Acad Sci USA 72:3235–3239.

659 23. Wadhwa N, Phillips R, Berg HC. 2019. Torque-dependent remodeling of the bacterial flagellar
660 motor. Proc Natl Acad Sci USA 201904577.

661 24. Pratt LA, Kolter R. 1998. Genetic analysis of *Escherichia coli* biofilm formation: roles of flagella,
662 motility, chemotaxis and type I pili. Mol Microbiol 30:285–293.

663 25. O'Toole GA, Kolter R. 1998. Flagellar and twitching motility are necessary for *Pseudomonas*
664 *aeruginosa* biofilm development. Mol Microbiol 30:295–304.

665 26. Bodenmiller D, Toh E, Brun YV. 2004. Development of surface adhesion in *Caulobacter*
666 *crescentus*. J Bacteriol 186:1438–1447.

667 27. Lauga E. 2016. Bacterial Hydrodynamics. Annu Rev Fluid Mech 48:105–130.

668 28. Shapiro L, Agabian-Keshishian N, Bendis I. 1971. Bacterial differentiation. Science 173:884–
669 892.

670 29. Poindexter JS. 1964. Biological properties and classification of the *Caulobacter* group. Bacteriol
671 Rev 28:231–295.

672 30. Degnen ST, Newton A. 1972. Chromosome replication during development in *Caulobacter*
673 *crescentus*. J Mol Biol 64:671–680.

674 31. Schmidt JM, Stanier RY. 1966. THE DEVELOPMENT OF CELLULAR STALKS IN BACTERIA. J Cell
675 Biol 28:423–436.

676 32. Poindexter JS. 1981. The caulobacters: ubiquitous unusual bacteria. Microbiol Rev 45:123–
677 179.

678 33. Hershey DM, Fiebig A, Crosson S. 2019. A Genome-Wide Analysis of Adhesion in *Caulobacter*
679 *crescentus* Identifies New Regulatory and Biosynthetic Components for Holdfast Assembly.
680 mBio 10:a000414-18.

681 34. Berne C, Ellison CK, Agarwal R, Severin GB, Fiebig A, Morton III RI, Waters CM, Brun YV. 2018.
682 Feedback regulation of *Caulobacter crescentus* holdfast synthesis by flagellum assembly via
683 the holdfast inhibitor HfiA. Mol Microbiol 9:e1003744-20.

684 35. Fiebig A, Herrou J, Fumeaux C, Radhakrishnan SK, Viollier PH, Crosson S. 2014. A Cell Cycle and
685 Nutritional Checkpoint Controlling Bacterial Surface Adhesion. PLoS Genet 10:e1004101-14.

686 36. Purcell EB, Siegal-Gaskins D, Rawling DC, Fiebig A, Crosson S. 2007. A photosensory two-
687 component system regulates bacterial cell attachment. Proc Natl Acad Sci U S A 104:18241–
688 18246.

689 37. Reyes Ruiz LM, Fiebig A, Crosson S. 2019. Regulation of bacterial surface attachment by a
690 network of sensory transduction proteins. PLoS Genet 15:e1008022.

691 38. Li G, Brown PJB, Tang JX, Xu J, Quardokus EM, Fuqua C, Brun YV. 2011. Surface contact
692 stimulates the just-in-time deployment of bacterial adhesins. Mol Microbiol 83:41–51.

693 39. Ellison CK, Kan J, Dillard RS, Kysela DT, Ducret A, Berne C, Hampton CM, Ke Z, Wright ER, Biais
694 N, Dalia AB, Brun YV. 2017. Obstruction of pilus retraction stimulates bacterial surface
695 sensing. Science 358:535–538.

696 40. Hug I, Deshpande S, Sprecher KS, Pfohl T, Jenal U. 2017. Second messenger–mediated tactile
697 response by a bacterial rotary motor. Science 358:531–534.

698 41. Sangermani M, Hug I, Sauter N, Pfohl T, Jenal U. 2019. Tad Pili Play a Dynamic Role in
699 *Caulobacter crescentus* Surface Colonization. mBio 10:740–18.

700 42. Dingwall A, Gober JW, Shapiro L. 1990. Identification of a *Caulobacter* basal body structural
701 gene and a cis-acting site required for activation of transcription. J Bacteriol 172:6066–6076.

702 43. Hershey DM, Porfírio S, Black I, Jaehrig B, Heiss C, Azadi P, Fiebig A, Crosson S. 2019.
703 Composition of the Holdfast Polysaccharide from Caulobacter crescentus. J Bacteriol
704 201:277–13.

705 44. Paul R, Weiser S, Amiot NC, Chan C, Schirmer T, Giese B, Jenal U. 2004. Cell cycle-dependent
706 dynamic localization of a bacterial response regulator with a novel di-guanylate cyclase
707 output domain. Genes Dev 18:715–727.

708 45. Leclerc G, Wang SP, Ely B. 1998. A new class of *Caulobacter crescentus* flagellar genes. J
709 Bacteriol 180:5010–5019.

710 46. Ellison CK, Rusch DB, Brun YV. 2019. Flagellar Mutants Have Reduced Pilus Synthesis in
711 *Caulobacter crescentus*. J Bacteriol 201:e00031-19.

712 47. Biondi EG, Skerker JM, Arif M, Prasol MS, Perchuk BS, Laub MT. 2006. A phosphorelay system
713 controls stalk biogenesis during cell cycle progression in *Caulobacter crescentus*. Mol
714 Microbiol 59:386–401.

715 48. Santiveri M, Roa-Eguiara A, Kühne C, Wadhwa N, Hu H, Berg HC, Erhardt M, Taylor NMI. 2020.
716 Structure and Function of Stator Units of the Bacterial Flagellar Motor. Cell 183:244-257.e16.

717 49. Deme JC, Johnson S, Vickery O, Aron A, Monkhouse H, Griffiths T, James RH, Berks BC, Coulton
718 JW, Stansfeld PJ, Lea SM. 2020. Structures of the stator complex that drives rotation of the
719 bacterial flagellum. Nat Microbiol https://doi.org/10.1038/s41564-020-0788-8.

720 50. Hosking ER, Vogt C, Bakker EP, Manson MD. 2006. The Escherichia coli MotAB Proton Channel
721 Unplugged. Journal of Molecular Biology 364:921–937.

722 51. Brenzinger S, Dewenter L, Delalez NJ, Leicht O, Berndt V, Paulick A, Berry RM, Thanbichler M,
723 Armitage JP, Maier B, Thormann KM. 2016. Mutations targeting the plug-domain of the *S*
724 *hewanella oneidensis* proton-driven stator allow swimming at increased viscosity and under
725 anaerobic conditions: MotB plug-domain mutants. Molecular Microbiology 102:925–938.

726 52. Wolfe AJ, Visick KL. 2008. Get the Message Out: Cyclic-Di-GMP Regulates Multiple Levels of
727 Flagellum-Based Motility. J Bacteriol 190:463–475.

728 53. Kaczmarczyk A, Hempel AM, Arx C, Böhm R, Dubey BN, Nesper J, Schirmer T, Hiller S, Jenal U.
729 2020. Precise timing of transcription by c-di-GMP coordinates cell cycle and morphogenesis
730 in Caulobacter. Nature Communications 1–16.

731 54. Duerig A, Abel S, Folcher M, Nicollier M, Schwede T, Amiot N, Giese B, Jenal U. 2009. Second
732 messenger-mediated spatiotemporal control of protein degradation regulates bacterial cell
733 cycle progression. Genes Dev 23:93–104.

734 55. Lori C, Ozaki S, Steiner S, Böhm R, Abel S, Dubey BN, Schirmer T, Hiller S, Jenal U. 2015. Cyclic
735 di-GMP acts as a cell cycle oscillator to drive chromosome replication. Nature 523:236–239.

736 56. Sprecher KS, Hug I, Nesper J, Potthoff E, Mahi M-A, Sangermani M, Kaever V, Schwede T,
737 Vorholt J, Jenal U. 2017. Cohesive Properties of the *Caulobacter crescentus* Holdfast Adhesin
738 Are Regulated by a Novel c-di-GMP Effector Protein. mBio 8:e00294-17–15.

739 57. Aldridge P, Paul R, Goymer P, Rainey P, Jenal U. 2003. Role of the GGDEF regulator PleD in
740 polar development of *Caulobacter crescentus*. Mol Microbiol 47:1695–1708.

741 58. Hecht GB, Newton A. 1995. Identification of a novel response regulator required for the
742 swarmer-to-stalked-cell transition in *Caulobacter crescentus*. J Bacteriol 177:6223–6229.

743 59. Zhou J, Sharp LL, Tang HL, Lloyd SA, Billings S, Braun TF, Blair DF. 1998. Function of
744 Protonatable Residues in the Flagellar Motor of *Escherichia coli*: a Critical Role for Asp 32 of
745 MotB. J Bacteriol 180:2729–2735.

746 60. Alberti L, Harshey RM. 1990. Differentiation of *Serratia marcescens* 274 into swimmer and
747 swarmer cells. J Bacteriol 172:4322–4328.

748 61. Kawagishi I, Imagawa M, Imae Y, McCarter L, Homma M. 1996. The sodium-driven polar
749 flagellar motor of marine *Vibrio* as the mechanosensor that regulates lateral flagellar
750 expression. Mol Microbiol 20:693–699.

751 62. Laventie B-J, Sangermani M, Estermann F, Manfredi P, Planes R, Hug I, Jaeger T, Meunier E,
752 Broz P, Jenal U. 2019. A Surface-Induced Asymmetric Program Promotes Tissue Colonization
753 by *Pseudomonas aeruginosa*. Cell Host Microbe 25:140-152.e6.

754 63. Laganenka L, López ME, Colin R, Sourjik V. 2020. Flagellum-Mediated Mechanosensing and
755 RflP Control Motility State of Pathogenic *Escherichia coli*. mBio 11:e02269-19.

756 64. Güvener ZT, Harwood CS. 2007. Subcellular location characteristics of the *Pseudomonas*
757 *aeruginosa* GGDEF protein, WspR, indicate that it produces cyclic-di-GMP in response to
758 growth on surfaces. Mol Microbiol 66:1459–73.

759 65. Luo Y, Zhao K, Baker AE, Kuchma SL, Coggan KA, Wolfgang MC, Wong GCL, O'Toole GA. 2015. A
760 Hierarchical Cascade of Second Messengers Regulates *Pseudomonas aeruginosa* Surface
761 Behaviors. mBio 6:73–11.

762 66. Belas R, Suvanasuthi R. 2005. The ability of *Proteus mirabilis* to sense surfaces and regulate
763 virulence gene expression involves FliL, a flagellar basal body protein. J Bacteriol 187:6789–
764 6803.

765 67. Tipping MJ, Delalez NJ, Lim R, Berry RM, Armitage JP. 2013. Load-dependent assembly of the
766 bacterial flagellar motor. mBio 4:1–6.

767 68. Partridge JD, Nieto V, Harshey RM. 2015. A New Player at the Flagellar Motor: FliL Controls
768 both Motor Output and Bias. mBio 6:77–11.

769 69. Hughes KT, Berg HC. 2017. The bacterium has landed. Science 358:446–447.

770 70. Wu DC, Zamorano-Sánchez D, Pagliai FA, Park JH, Floyd KA, Lee CK, Kitts G, Rose CB, Bilotta
771 EM, Wong GCL, Yildiz FH. 2020. Reciprocal c-di-GMP signaling: Incomplete flagellum
772 biogenesis triggers c-di-GMP signaling pathways that promote biofilm formation. PLoS Genet
773 16:e1008703.

774 71. Harrison JJ, Almblad H, Irie Y, Wolter DJ, Eggleston HC, Randall TE, Kitzman JO, Stackhouse B,
775 Emerson JC, Mcnamara S, Larsen TJ, Shendure J, Hoffman LR, Wozniak DJ, Parsek MR. 2020.
776 Elevated exopolysaccharide levels in *Pseudomonas aeruginosa* flagellar mutants have
777 implications for biofilm growth and chronic infections. PLoS Genet 16:e1008848.

778 72. Radhakrishnan SK, Thanbichler M, Viollier PH. 2008. The dynamic interplay between a cell fate
779 determinant and a lysozyme homolog drives the asymmetric division cycle of *Caulobacter*
780 *crescentus*. Genes Dev 22:212–225.

781 73. Janakiraman B, Mignolet J, Narayanan S, Viollier PH, Radhakrishnan SK. 2016. In-phase
782 oscillation of global regulons is orchestrated by a pole-specific organizer. Proc Natl Acad Sci U
783 S A 113:12550–12555.

784 74. Mignolet J, Holden S, Bergé M, Panis G, Eroglu E, Théraulaz L, Manley S, Viollier PH. 2016.
785 Functional dichotomy and distinct nanoscale assemblies of a cell cycle-controlled bipolar
786 zinc-finger regulator. eLife 5:e20640-21.

787 75. Tan MH, Kozdon JB, Shen X, Shapiro L, McAdams HH. 2010. An essential transcription factor,
788 SciP, enhances robustness of *Caulobacter* cell cycle regulation. Proc Natl Acad Sci U S A
789 107:18985–18990.

790 76. Anderson DK, Ohta N, Wu J, Newton A. 1995. Regulation of the *Caulobacter crescentus rpoN*
791 gene and function of the purified σ54 in flagellar gene transcription. Mol Gen Genet 246:697–
792 706.

793 77. Aldridge P, Jenal U. 1999. Cell cycle-dependent degradation of a flagellar motor component
794 requires a novel-type response regulator. Mol Microbiol 32:379–391.

795 78. Baker AE, Webster SS, Diepold A, Kuchma SL, Bordeleau E, Armitage JP, O'Toole GA. 2019.
796 Flagellar Stators Stimulate c-di-GMP Production by *Pseudomonas aeruginosa*. J Bacteriol
797 201:263–13.

798 79. Toutain CM, Zegans ME, O'Toole GA. 2005. Evidence for Two Flagellar Stators and Their Role
799 in the Motility of *Pseudomonas aeruginosa*. J Bacteriol 187:771–777.

800 80. Quon KC, Marczynski GT, Shapiro L. 1996. Cell Cycle Control by an Essential Bacterial Two-
801 Component Signal Transduction Protein. Cell 84:83–93.

802 81. Kaczmarczyk A, Hempel AM, von Arx C, Böhm R, Dubey BN, Nesper J, Schirmer T, Hiller S, Jenal
803 U. 2020. Precise timing of transcription by c-di-GMP coordinates cell cycle and
804 morphogenesis in *Caulobacter*. Nat Commun 11:816.

805 82. Gibson DG, Young L, Chuang R-Y, Venter JC, Hutchison CA, Smith HO. 2009. Enzymatic
806 assembly of DNA molecules up to several hundred kilobases. Nat Methods 6:343–345.

807 83. Ely B. 1991. Genetics of Caulobacter crescentus. Meth Enzymol 204:372–384.

808 84. Thanbichler M, Iniesta AA, Shapiro L. 2007. A comprehensive set of plasmids for vanillate- and
809 xylose-inducible gene expression in *Caulobacter crescentus*. Nucleic Acids Res 35:e137–e137.

810 85. Wetmore KM, Price MN, Waters RJ, Lamson JS, He J, Hoover CA, Blow MJ, Bristow J, Butland G,
811 Arkin AP, Deutschbauer A. 2015. Rapid Quantification of Mutant Fitness in Diverse Bacteria
812 by Sequencing Randomly Bar-Coded Transposons. mBio 6:e00306-15–15.

813 86. Kent WJ. 2002. BLAT—The BLAST-Like Alignment Tool. Genome Res 12:656–64.

814 87. Barrick JE, Colburn G, Deatherage DE, Traverse CC, Strand MD, Borges JJ, Knoester DB, Reba A,
815 Meyer AG. 2014. Identifying structural variation in haploid microbial genomes from short-
816 read resequencing data using breseq. BMC Genomics 15:1039.

817 88. Soding J, Biegert A, Lupas AN. 2005. The HHpred interactive server for protein homology
818 detection and structure prediction. Nucleic Acids Research 33:W244–W248.

819 89. Kelley LA, Mezulis S, Yates CM, Wass MN, Sternberg MJE. 2015. The Phyre2 web portal for
820 protein modeling, prediction and analysis. Nat Protoc 10:845–858.

821

822

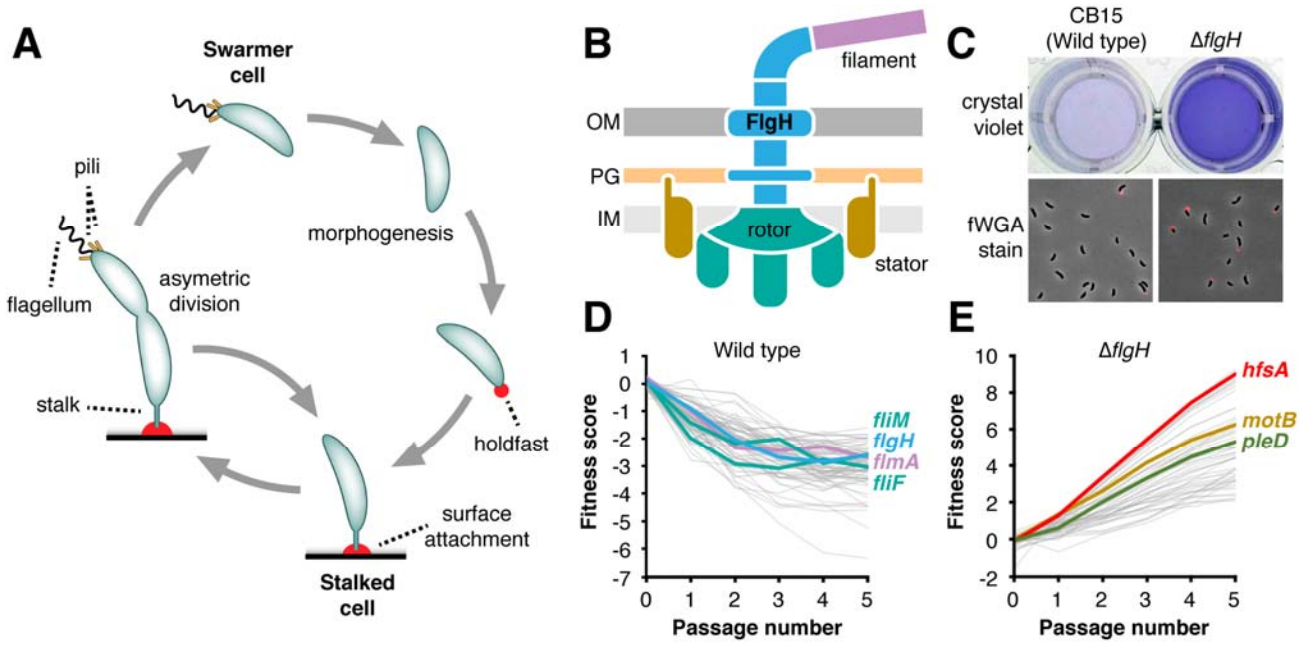

823

824 **Figure 1** *Identifying genes that link the flagellum to holdfast production*

825 A) The asymmetric division cycle of *C. crescentus*. Sessile stalked cells divide to release a newborn
826 swarmer cell that displays a flagellum and type IV pili. Quiescent swarmer cells undergo a
827 morphological transition to become replication competent stalked cells. Transitioning swarmer
828 cells can make an adhesin called the holdfast (red) that promotes surface attachment. B)
829 Schematic of flagellar architecture. A central hook-basal body (HBB) complex (blue) spanning the
830 cell envelope tethers a long extracellular filament (purple) to the surface of the cell. Multiple stator
831 subunits (gold) that surround the inner membrane embedded rotor (teal) use ion translocation to
832 turn the HBB and its associated filament. Outer membrane (OM), peptidoglycan (PG) and inner
833 membrane (IM) layers of the envelope are shown. C) The Δ*flgH* mutant shows increased surface
834 colonization (top), as measured by crystal violet (CV) staining, and a higher proportion of holdfast
835 producing cells relative to wild type (bottom). Holdfasts were stained with Alexa 594-wheat germ
836 agglutinin (fWGA). D) Hyper-adhesive mutants identified by adhesion profiling in defined
837 medium. The 75 genes with the strongest hyper-adhesive profiles are plotted, and specific

838 flagellar assembly genes are highlighted. Colors correspond to the structural proteins depicted in
839 panel B. The plotted genes are listed in Table S1. E) The *flagellar signaling suppressor* (*fss*) genes
840 identified by adhesion profiling in the Δ*flgH* background. The 50 genes with the strongest
841 contributions to adhesion in the Δ*flgH* background are plotted. *hfsA*, a gene required for holdfast
842 biosynthesis, is highlighted along with two *fss* genes, *pleD* and *motB.* The plotted genes are listed in
843 Table S2. For panels D and E, each line represents the average fitness values for a single gene
844 plotted as a function of time in the sequential passaging experiment. Hyper-adhesive mutants are
845 depleted more rapidly than neutral mutants during selection in cheesecloth. Mutated genes (*fli*, *flg,*
846 *flm*, etc.) that display increased attachment to cheesecloth show steadily decreasing fitness scores
847 as a function of passage number. Mutants with reduced adhesion are enriched in broth when
848 grown with cheesecloth. Mutated genes that display decreased adhesion (*hfs* and *fss*) show
849 steadily increasing fitness scores.
850

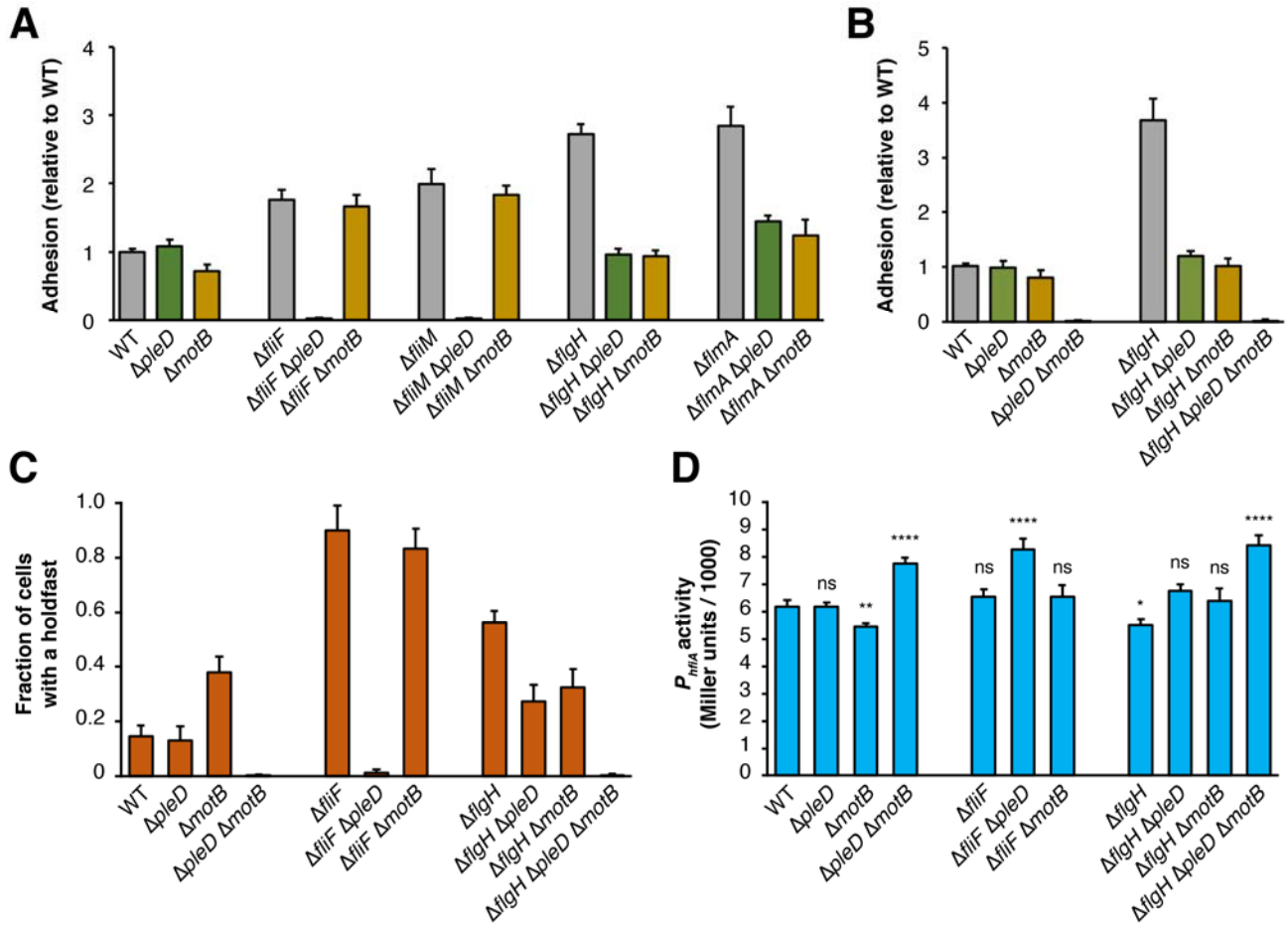

Figure 2 *Two distinct signaling pathways operate downstream of the flagellum to control adhesion*

A) Crystal violet-based attachment assay showing suppression of the hyper-adhesive phenotypes by *pleD* and *motB* in early (Δ*fliF* and Δ*fliM*) and late (Δ*flgH* and Δ*flmA*) flagellar assembly mutants. Mean values from six biological replicates are shown with error bars representing the associated standard deviations. B) Crystal violet-based attachment assay showing the additive effects of Δ*motB* and Δ*pleD* on adhesion in the WT and Δ*flgH* backgrounds. Mean values from five biological replicates are shown with the associated standard deviations. C) Fraction of cells with a holdfast in flagellar mutant and suppressor backgrounds. Holdfasts were stained and counted from log phase cultures as described in Materials and Methods. D) *hfiA* transcription in flagellar mutant and suppressor backgrounds as measured by beta-galactosidase activity from a P_{hfiA}-*lacZ* reporter. Mean values from three biological replicates collected on two separate dates for a total of six replicates are shown with the associated standard deviations. Statistical significance was

evaluated with ANOVA followed by Tukey's multiple comparison test. Significance compared to wild-type is indicated above each bar. (ns): not significant; (*): $P < 0.1$; (**): $P < 0.01$; (****): $P < 0.0001$. A full statistical analysis of the CV staining, holdfast count and LacZ activity measurements is reported in Table S3.

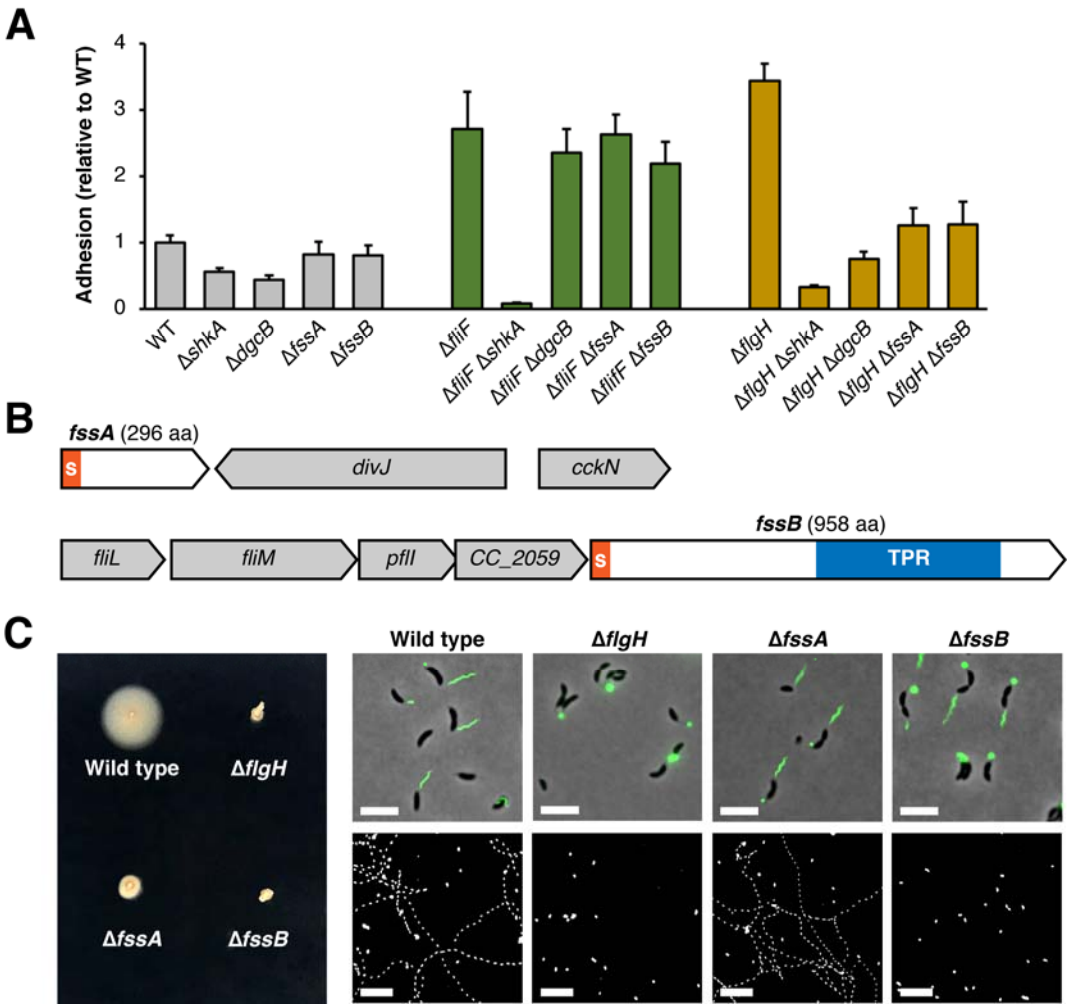

Figure 3 *Two novel motility genes contribute to activation of the mechanical pathway*

A) Crystal violet-based attachment assay evaluating suppression of early and late flagellar assembly mutants by individual *fss* genes. Mean values from six biological replicates are shown with error bars representing the associated standard deviations. B) Genomic context of the *fssA* and *fssB* genes. Orange S: secretion signal; blue bar: tetratricopeptide repeat region. C) Motility phenotypes of the Δ*fssA* and Δ*fssB* mutants. Left: soft-agar motility assay. Top right: flagellar filaments stained with Alexa488-maleimide after introduction of the *fljK*^{T103C} allele into the indicated mutants. Note that the maleimide dye cross-reacts with holdfast. Scale bars represent 5μm. Bottom right: maximum projections from time-lapse microscopy. Cells appear in white, and tracks for motile cells appear as dotted lines. Scale bars represent 25μm.

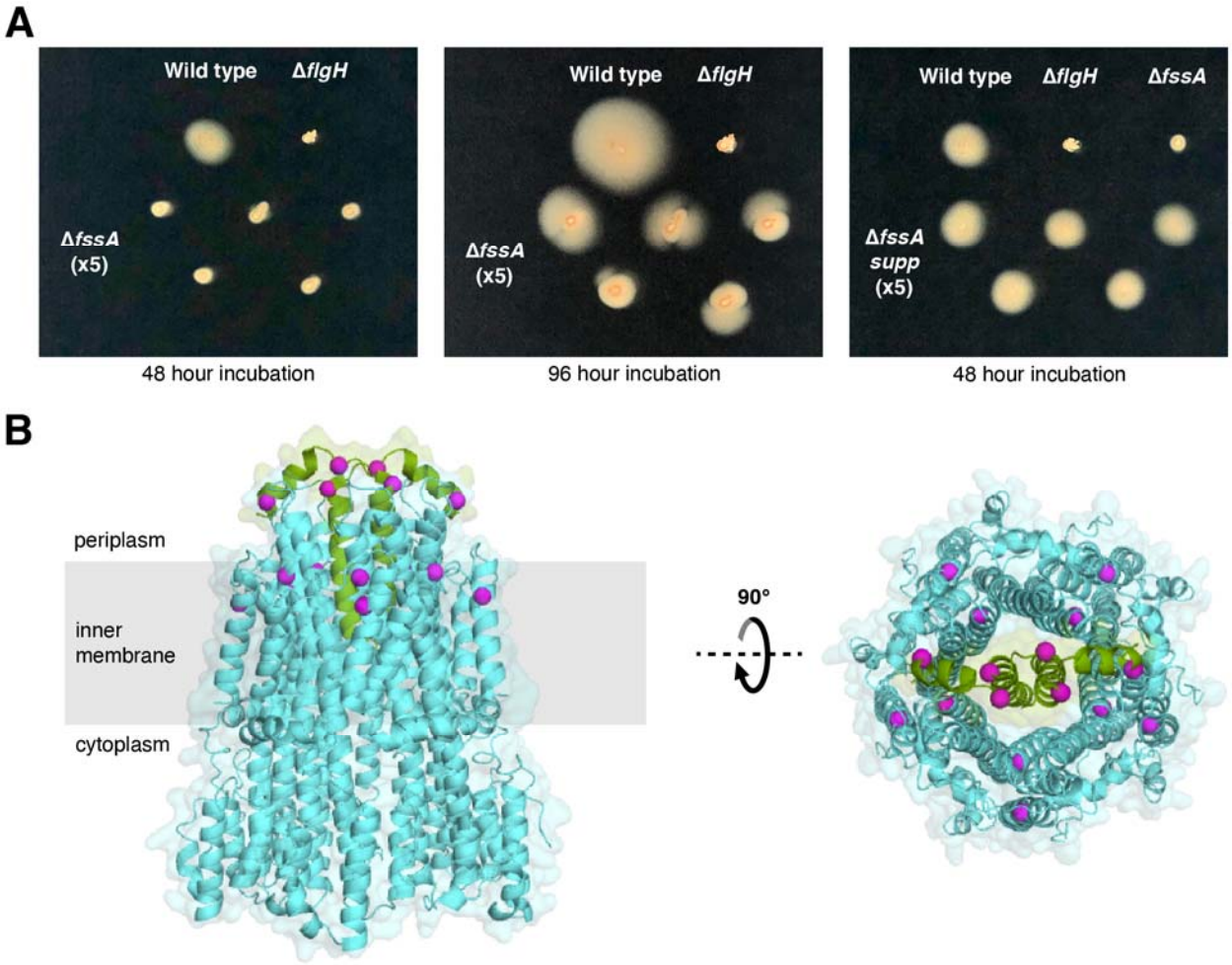

Figure 4 *Suppression of the Δ*fssA *motility phenotype by second site mutations in the stator genes*

A) Soft-agar motility assays showing the emergence of motile flares after prolonged incubation of the Δ*fssA* mutant. Single colonies isolated from the leading edge of flares (middle image) displayed wild-type motility when reinoculated into soft-agar (right image). B) Mapping of Δ*fssA* suppressors onto a homology model of the *C. crescentus* stator. Mutations are located at the periplasmic face of the complex. Identification of multiple mutations in the "plug" region of MotB suggests that the suppressing mutations activate ion translocation ectopically.

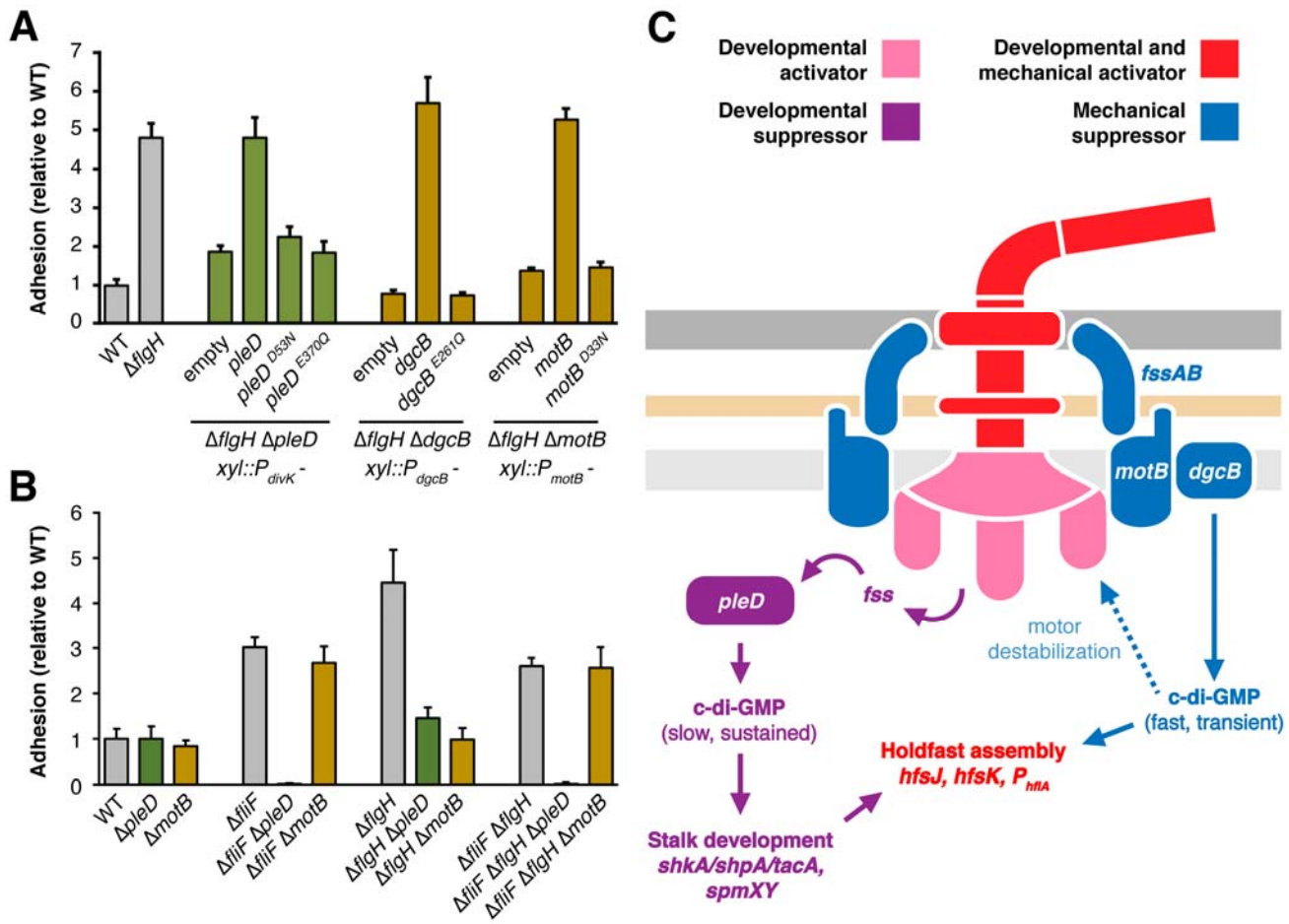

Figure 5 *Convergence of flagellar signaling on cyclic-di-GMP*

A) Crystal violet-based attachment assay showing that inactive alleles of *fss* genes in the developmental (*pleD*) and mechanical (*dgcB* and *motB*) pathways do not support flagellar signaling. Each allele is expressed from the gene's native promoter and integrated as a single copy at the *xylX* locus. The genotype and promoter for each strain are indicated below the solid line. Mean values from seven biological replicates are shown with error bars representing the associated standard deviations. B) Crystal violet-based attachment assay showing that early flagellar mutants are epistatic to late flagellar mutants for activation of the mechanical pathway. The Δ*fliF* Δ*flgH* strain phenocopies the Δ*fliF* strain and demonstrates that the effect of *motB* on adhesion requires early stages of flagellar assembly. Mean values from five biological replicates are shown with the associated standard deviations. C) Two signaling pathways operate downstream of the flagellum in *C. crescentus.* We propose that mechanical signals are transmitted

901 through the motor to activate DgcB, producing a transient burst of c-di-GMP synthesis that
902 directly activates holdfast biosynthesis enzymes. Persistent filament obstruction activates PleD by
903 destabilizing the motor and triggering flagellar disassembly. PleD activation through this
904 mechanism is predicted to induce sustained c-di-GMP production and initiation of the
905 transcriptional program that leads to stalk development.
906

907 **Supplemental materials**

908 ***Table S1*** *Mutated genes that produce a hyper-adhesive phenotype during adhesion profiling* Mean
909 fitness scores for each successive passage (P1-P5) of the barcoded CB15 Tn-Himar mutant library
910 in cheesecloth are shown along with a nonselective control (P0). Negative values indicate hyper-
911 adhesive strains that are depleted more rapidly than the bulk population.

912 ***Table S2*** *Mutated genes that suppress hyper-adhesion in the Δ*flgH *background during adhesion*
913 *profiling* Mean fitness scores for each successive passage (P1-P5) of the barcoded Δ*flgH* Tn-Himar
914 mutant library in cheesecloth are shown along with a nonselective control (P0). Positive values
915 indicate strains with reduced adhesion that are depleted less rapidly than the bulk population.

916 ***Table S3*** *Statistical analysis of strain comparisons shown in Figure 2*

917 The results of ANOVA followed by Tukey's multiple comparison test for 11 critical strains in Fig 2
918 is shown. Adjusted P values for each comparison are highlighted in blue, and statistical
919 significance is highlighted in green. (*) – P < 0.05; (**) – P < 0.01; (***) – P < 0.001; (****) – P <
920 0.0001.

921 ***Table S4*** *Plasmids used in this study*

922 ***Table S5*** *Strains used in this study*

923 ***Table S6*** *Features of the barcoded transposon libraries used in this study*

924 ***Figure S1*** *Surface contact independent activation of holdfast production in Δ*flgH A) Shedding of
925 holdfast polysaccharide into spent medium. Δ*flgH* releases a holdfast specific fWGA reactive
926 material into the spent medium during growth in M2X liquid. B) Comparison showing the fraction
927 of holdfast producing cells in wild type and Δ*flgH* backgrounds. Centrifugation has no effect on
928 holdfast production in either strain. C) Micrographs of wild type and Δ*flgH* mutant cells taken
929 immediately after direct staining of holdfast in liquid cultures.

930 ***Figure S2*** *Confirmation of the two-pathway model for flagellar control of holdfast production* A) CV
931 staining of mutants from Fig2D grown in PYE. The loss of adhesion when the mechanical (Δ*motB*)
932 and developmental (Δ*pleD*) pathways are inactivated simultaneously is not specific to defined
933 M2X medium. Mean values from six biological replicates are shown along with their associated
934 standard deviations. B) CV stain confirming the placement of *motA* in the mechanical pathway.
935 Δ*motA* reduces hyper-adhesion specifically in late flagellar mutants, mirroring the Δ*motB*
936 suppression pattern. Mean values from seven biological replicates are shown along with their
937 associated standard deviations. C) CV stain showing additive effects of disrupting *shkA* and *motB*
938 simultaneously. The results confirm the placement of *shkA* and *motB* in separate signaling
939 pathways. Mean values from six biological replicates are shown along with their associated
940 standard deviations. D) CV stain showing additive effects of disrupting *shkA* and *dgcB*
941 simultaneously. The results confirm the placement of *shkA* and *dgcB* in separate signaling
942 pathways. Mean values from six biological replicates are shown along with their associated
943 standard deviations.
944 ***Figure S3*** *Additional analysis of the Δ*fssA *phenotype* A) Mapping of mutations that suppress the
945 Δ*fssA* motility phenotype by whole genome sequencing. The suppressor numbers correspond to
946 files in SRA accession PRJNA672134. Nucleotide positions correspond to coordinates in the
947 NA1000 genome. B) Soft-agar motility assay showing that the Δ*fssB* motility defect is epistatic to
948 the Δ*fssA* phenotype. Motile suppressors do not appear in the Δ*fssA* Δ*fssB* double mutant after a 96
949 hour incubation. C) CV staining experiment showing that the Δ*fssA* and Δ*fssB* are not additive for
950 suppression of hyper-adhesion in the Δ*flgH* mutant. Mean values from six biological replicates are
951 shown along with their associated standard deviations.
952 ***Figure S4*** *Genetic complementation of surface attachment and motility phenotypes* A)
953 Complementation of flagellar hierarchy mutants in soft agar. B) Complementation of hyper-

954 adhesion in flagellar mutants. C) Complementation of crystal violet staining for *fss* mutants in

955 Δ*flgH* background. D, E) Restoration of motility phenotypes in soft agar for *fss* mutants.